Cancer Immunology, Immunotherapy (2023) 72:969–984
https://doi.org/10.1007/s00262-022-03306-1

RESEARCH

αVEGFR2-MICA fusion antibodies enhance immunotherapy effect and synergize with PD-1 blockade

Mingzhu Pan[1] · Fei Wang[1] · Lidi Nan[1] · Siyu Yang[1] · Jinyao Qi[1] · Jiajun Xie[1] · Shuai Shao[1] · Hongyi zou[1] · Min Wang[1] · Fumou Sun[2] · Juan Zhang[1]

Received: 20 March 2022 / Accepted: 6 October 2022 / Published online: 13 October 2022

Abstract

Antiangiogenic therapy has shown significant clinical benefits in gastric cancer (GC) and non-small cell lung cancer (NSCLC). However, their effectiveness is limited by the immunosuppressive tumor microenvironment. The MHC class I chain-related molecules A and B (MICA/B) are expressed in many human cancers, enabling elimination of cancer cells by cytotoxic lymphocytes through natural killer group 2D (NKG2D) receptor activation. To improve antiangiogenic therapy and prolong its efficacy, we generated a bi-specific fusion protein (mAb04-MICA). This was comprised of an antibody targeting VEGFR2 fused to a MICA α1–α2 ectodomain. mAb04-MICA inhibited proliferation of GC and NSCLC cells through specific binding to VEGFR2 and had superior anti-tumor efficacy in both GC and NSCLC-bearing mouse models compared with ramucirumab. Further investigation revealed that the mAb04-MICA promoted NKG2D$^+$ NK cell activation and induced the tumor-associated macrophage (TAM) polarization from M2 type to M1 type both in vitro and in vivo. The polarization of TAMs upon NKG2D and MICA mediated activation has not yet been reported. Moreover, given the up-regulation of PD-L1 in tumors during anti-angiogenesis therapy, anti-PD-1 antibody enhanced the anti-tumoral activity of mAb04-MICA through stimulating infiltration and activation of NKs and CD8$^+$T cells in responding tumors. Our findings demonstrate that dual targeting of angiogenesis and NKG2D, or in combination with the PD-1/PD-L1 blockade, is a promising anti-tumor therapeutic strategy. This is accomplished through maintaining or reinstating tumor immunosurveillance during treatment, which expands the repertoire of anti-angiogenesis-based cancer immunotherapies.

Keywords Immunotherapy · MICA · VEGFR2 · Macrophage · NK cells

Introduction

Epithelial cancers such as gastric cancer (GC) and non-small cell lung cancer (NSCLC) are highly malignant and have a poor prognosis [1–3]. Angiogenesis is a fundamental process for sustaining the solid tumors microenvironment, tumor growth, and metastasis [4, 5]. Vascular endothelial growth factor (VEGF) ligands and their receptors (VEGFR2) play a central role in these processes. Therefore, inhibition of VEGF-VEGFR2 signaling becomes a novel and attractive therapeutic strategy in malignant tumors [1–3].

Ramucirumab (LY3009806), an antiangiogenic agent, has been approved for second-line therapy in GC and NSCLC [6–8]. Like other antiangiogenic drugs, side effects like hypertension, gastrointestinal perforation, and bleeding have been attributed to the excessive suppression of VEGF/VEGFR2 [9–11]. Importantly, the up-regulation of adaptive immunosuppressive pathways leads to drug resistance during antiangiogenic therapy, despite the presence of tumor-infiltrating lymphocytes [12]. To address these issues, a combination of anti-programmed cell death protein 1 (PD-1) and antiangiogenic antibodies was investigated against solid tumors in clinical trials. However, many patients failed to

Mingzhu Pan and Fei Wang have contributed equally to this work.

✉ Fumou Sun
fsun@uams.edu

✉ Juan Zhang
zhangjuan@cpu.edu.cn

[1] Antibody Engineering Laboratory, School of Life Science and Technology, China Pharmaceutical University, Nanjing 211198, China

[2] Department of Internal Medicine, Myeloma Center, Winthrop P. Rockefeller Cancer Institute, University of Arkansas for Medical Sciences, Little Rock, AR 72205, USA

respond to PD-1 blockade and late relapses are now emerging [13]. We, herein, hypothesize dual-targeting VEGFR2 and activating receptors of innate immune systems, such as NK cells and macrophages, can reverse the tumor immunosuppressive microenvironment and sensitize tumors to antiangiogenic therapy and prolong its efficacy.

The activation of NK cells is regulated by a balance between activating receptors and inhibitory receptors [14, 15]. One of the most important activating receptors for NK cells is natural killer group 2D (NKG2D) [16, 17]. NKG2D mediates anti-tumor activity mainly through ligand MHC class I chain-related protein A (MICA), which is generally expressed on tumor cells but not normal cells [18, 19]. However, tumor cells evade NK cell-mediated immune surveillance through shedding MICA [20–22]. Thus, discovery of a new approach to remodeling the immune surveillance of NK cells would be critical for eliminating tumors.

NKG2D is also found expressed on activated macrophages [23]. Because of their plasticity and heterogeneity, macrophages can be generated with two different phenotypes, tumoricidal M1 macrophages and pro-tumorigenic M2 macrophages [24]. The M2 tumor-associated macrophage (TAM) is an immunosuppressive cell that contributes to the growth and metastasis of tumor cells [25]. The main strategy for targeting TAMs is to increase tumoricidal M1 type and to decrease pro-tumor M2 type [26]. We suspect that activation of NKG2D on macrophages may be relevant to the polarization of TAMs. We previously generated a bi-specific fusion protein, comprised of full-length human anti-VEGFR2 antibody and MICA (mAb04-MICA), which displayed antineoplastic activity through VEGFR2 and NKG2D targeting [27], we have further investigated the efficacy of mAb04-MICA against GC and NSCLC, both in vitro and in vivo, and explored potential therapeutic mechanisms on the tumor-immune microenvironment (TIME). Furthermore, since PD-L1 is up-regulated in tumor tissues during anti-angiogenesis therapy, we investigated the synergistic anti-tumor activity of mAb04-MICA with the anti-PD-1 antibody.

Materials and methods

Cell culture

Normal human liver cell line HL-7702, human GC cell lines BGC-823 were purchased from Cell Bank of the Chinese Academy of Science. Kidney HEK-293, mouse macrophage RAW264.7, human GC cell lines AGS, NSCLC cell lines H157/H1299/H1975, murine Lewis lung carcinoma cell line (LLC), and the NK cell line NK-92 were obtained from American Type Culture Collection. These cells were preserved in our laboratory and maintained in RPMI 1640 medium or DMEM medium with 10% FBS(Gibco). The NK cell line NK-92 was cultured in supplemented MEM Alpha Medium (Gibco), 12.5% FBS (Hyclone), 12.5% horse serum (Hyclone), 0.1 mM 2-Mercaptoethanol, 0.2 mM Myo-inositol (Sigma), 0.02 mM Folic Acid (Sigma), and 200 U/mL hIL-2 (Millipore).

Animals and antibodies

Six-week female BALB/c nude mice and C57BL/6 mice were purchased from Comparative Medicine Centre of Yangzhou University (China). Six-week female NOD-SCID mice were purchased from Junke Bioengineering Co. (China). All animals were treated following the standards of China Pharmaceutical University. The Chinese hamster ovary (CHO) cell line contained the plasmid of mAb04, mAb04-MICA, anti-PD-1 antibody JZD00 was constructed by our laboratory and maintained in DMEM/F12 medium (Gibco) with 10% FBS. The culture supernatants were collected to purify fusion antibodies by a Protein A affinity chromatography column (GE Healthcare, Buckinghamshire, UK). Anti-VEGFR2-MICA bi-specific antibody (AK404-MICA) consists of MICA and an anti-VEGFR2 single-chain antibody fragment (AK404) expressed in Pichia pastoris X-33 and was purified by nickel column chromatography [28]. Ramucirumab was presented by Alphamab (China). PBMC from a healthy donor and inform the purpose of the experiment.

The construction of shVEGFR2 BGC-823 and H157 cell lines

DNA oligo against VEGFR2 gene (5'-CCGGGTGCTGTT TCTGACTCC TAATCTCGAGATTAGGAGTCAGAAACA GCACTTTTTG-3') was cloned into pLKO.1-puro shRNA vector (Addgene) [29]. Plasmid DNA including sh-VEGFR2 (sh-VR2) or non-targeting shRNA (sh-control) was transfected into BGC-823 or H157 cells along with envelope and packaging vector to produce lentivirus packed with shRNA cassettes using the standard procedure, respectively. After transfection, sh-VR2 BGC-823 or H157 cells and sh-control BGC-823 or H157 cells were cultured in the presence of 2 μg/mL puromycin to achieve stable cell lines.

Cell proliferation, apoptosis, and cell cycle analysis

Tumor cells (4×10^3/well) were seeded in 96-well plates and incubated with different concentrations of mAb04-MICA/mAb04/ramucirumab (0.4,2,10,50,100,200 nM) at 37 °C for 72 h. Cell viability was quantitated by an MTT assay. Inhibition(%) = (1- $OD_{experiment}/OD_{control}$) × 100%.

Tumor cells were cultured at 2×10^5/well in 6-well plates for 24 h and incubated with mAb04 or mAb04-MICA

(200 nM) at 37 ℃ for 72 h. The cells were harvested and stained with annexin V-FITC and propidium iodide (PI) using an Apoptosis Assay Kit (Sangon Biotech).

The cells were harvested and fixed with absolute ethanol for 24 h and stained with PI (Beyotime Biotech). The proportion of singlet cells in G0/G1, S, and G2 were calculated with MFLT32 software.

Western blot assay

Tumor cells were serum-starved for 12 h, then treated with mAb04-MICA (200 nM) for 1 h and induced with $VEGF_{165}$(10 ng/mL) for another 1 h. The cells were harvested, and whole protein was extracted using RAPI buffer (Beyotime). The influence of mAb04-MICA on the phosphorylation of VEGFR2/AKT/ERK/P38 MAPK was examined (Cell Signaling). Expression of Bcl2/Bcl-xL/Bak/Bax was analyzed to determine apoptotic activity.

RAW264.7 cells were co-cultured with LLC for 24 h with AK404R or AK404R-MICA (1000 nM). The positive control was set as 5 ng/mL IFN-γ + 100 ng/mL LPS (Solarbio) group or 10 ng/mL IL-4 (Solarbio) group which can induce RAW264.7 to express different functional markers of M1 or M2 macrophages and the induction was performed for 48 h before use. Anti-CD16/32 or anti-CD206 antibodies (BioLegend) were used to detect the polarization of RAW264.7.

Cytotoxicity assay

Tumor cells were co-cultured with various amounts of NK-92 cells, PBMCs, or RAW264.7 cells and 200 nM mAb04/mAb04-MICA/mAb04-MICA or 1000 nM AK404R/ AK404R-MICA for 4 h. The ratios of PBMCs: tumor cells were 5:1, 30:1, and 100:1, and the ratios of NK-92/RAW264.7: tumor cells were 1:1, 5:1, and 10:1. 50 μL supernatants were then analyzed for the activity using an LDH Assay Kit (YEASEN). Controls were set as groups of spontaneous LDH release in effector or target cells, and as a group to target maximum release. Cell lysis(%) = 100 × ([Experimental—Effector Spontaneous—Target Spontaneous] / [Target Maximum—Target Spontaneous]).

Degranulation and assay of cytokine production of NK-92 cells

NK-92 cells were incubated with 1000 U/mL IL-2 for 24 h and co-incubated with GC cells for 4 h at an effector/target (E/T) ratio of 10:1. The concentrations of mAb04, mAb04-MICA, and soluble MICA were 200 nM. The degranulated NK cells were detected by flow based on the release of CD107a [30]. Then, the supernatant was collected, and the secreted IFN-γ and TNF-α were detected using ELISA kits (KeyGEN Biotech). To assess the expression levels of intracellular granzyme B and perforin, membranes of the co-cultured cells were ruptured by treatment with Inside Fix/Inside Perm (Miltenyi), followed by incubation with anti-granzyme B-PE/anti-perforin-FITC antibody. Cells were analyzed by flow.

Xenograft model and administration

1×10^7 tumor cells were injected subcutaneously into the left armpit of BALB/c nude mice or C57BL/6 mice. When average tumor volume reached 100 mm^3, the tumor-bearing mice were divided randomly into groups (5/group) and treated with indicated treatments by intravenous injection every 3 d (BALB/c nude mice) or 2 d (C57BL/6 mice). In the BGC-823-bearing nude mouse model, there were six groups: Control, mAb04-MICA (5 mg/kg), mAb04 (5 mg/kg), ramucirumab (5 mg/kg), mAb04-MICA (5 mg/kg) + docetaxel (10 mg/kg), and ramucirumab (5 mg/kg) + docetaxel (10 mg/kg). In the H157-bearing nude mouse model, there were five groups: Control, mAb04-MICA (10 mg/kg), mAb04 (10 mg/kg), mAb04-MICA (10 mg/kg) + docetaxel (2 mg/kg), and ramucirumab (10 mg/kg) + docetaxel (2 mg/kg). In the H1975-bearing nude mouse model or NOD-SCID mouse model, there were four group: Control, mAb04-MICA (10 mg/kg), JZD00 (10 mg/kg), and mAb04-MICA (10 mg/kg) + JZD00 (10 mg/kg). All nude mice were injected with 1×10^7 human PBMC intravenously at day 2 after tumor inoculation, and once every 6 days thereafter. NOD-SCID mice were injected with PBMC intravenously at the same time of tumor inoculation. In the LLC-bearing C57BL/6 mouse model, the doses of AK404R-MICA and AK404R were 2 mg/kg. Tumor development was measured every 2 d. The mice were sacrificed 19 d (nude mice) or 15 d (C57BL/6 mice) after treatments, and tumor tissues were prepared for further analysis.

Detection of the proportion and activation of tumor-associated immune cells by flow cytometry

Mice were sacrificed after administration for 8–12 d. Tumors were collected, and ground into single cells by a 200-mesh screen. Tumor-infiltrating lymphocytes (TILs) and macrophages were isolated using Percoll centrifugation media (Tbdscience). The proportion of activated $CD8^+$T cells, NK cells, and macrophages in the tumor tissues were detected by flow cytometry. The details of antibodies used in this study are listed in supplementary table 1.

Immunohistochemistry and immunofluorescence

Immunohistochemical (IHC) analysis was performed using antibodies against Ki-67, VEGF, CD31, CD8, CD4,

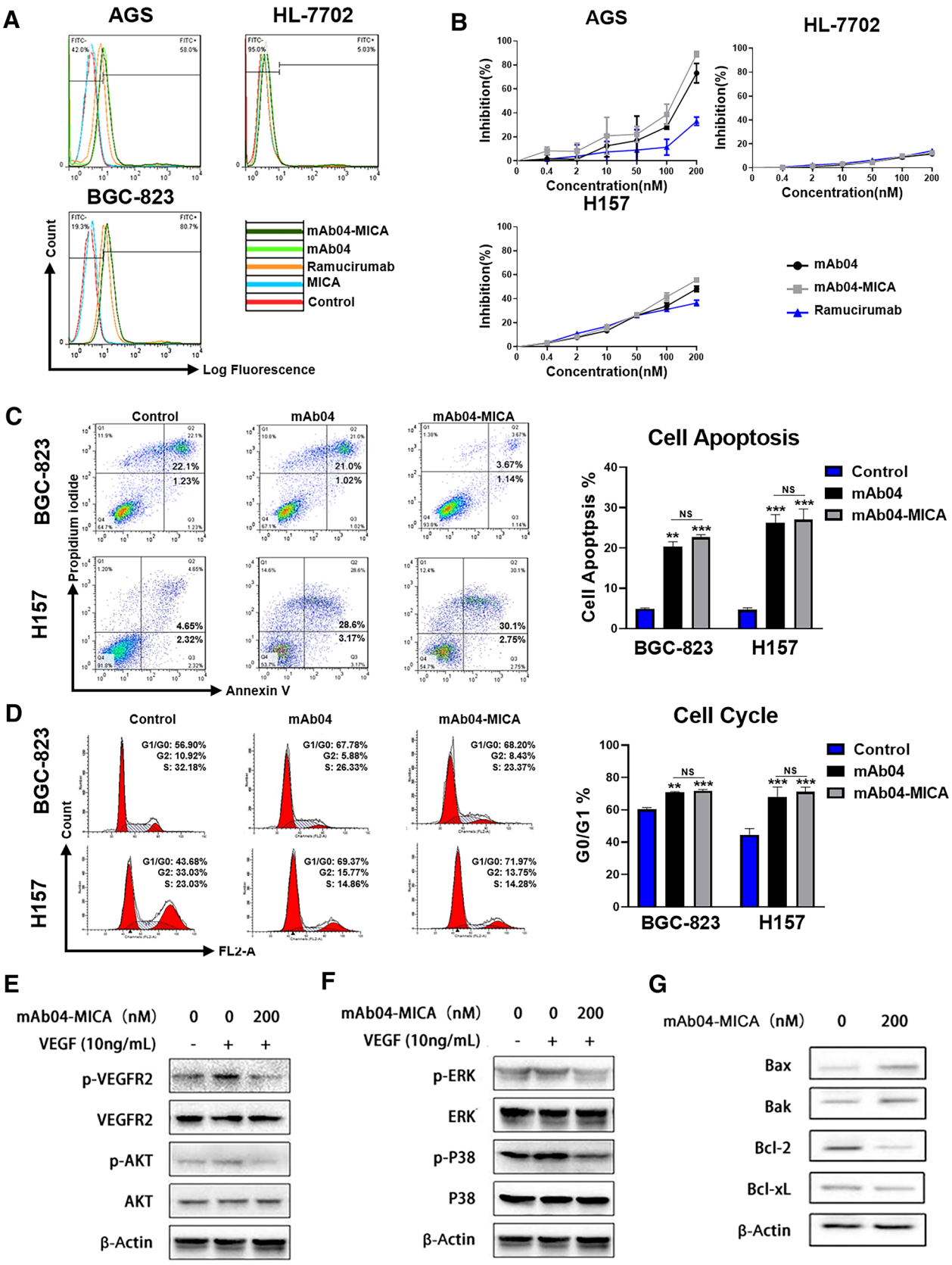
A
AGS
HL-7702
BGC-823
Count
Log Fluorescence
mAb04-MICA
mAb04
Ramucirumab
MICA
Control
B
AGS
HL-7702
H157
Inhibition(%)
Concentration(nM)
mAb04
mAb04-MICA
Ramucirumab
C
Control
mAb04
mAb04-MICA
BGC-823
H157
Propidium Iodide
Annexin V
22.1%
1.23%
21.0%
1.02%
3.67%
1.14%
4.65%
2.32%
28.6%
3.17%
30.1%
2.75%
Cell Apoptosis
Cell Apoptpsis %
NS
**
***
Control
mAb04
mAb04-MICA
BGC-823
H157
D
Control
mAb04
mAb04-MICA
BGC-823
H157
Count
FL2-A
G1/G0: 56.90%
G2: 10.92%
S: 32.18%
G1/G0: 67.78%
G2: 5.88%
S: 26.33%
G1/G0: 68.20%
G2: 8.43%
S: 23.37%
G1/G0: 43.68%
G2: 33.03%
S: 23.03%
G1/G0: 69.37%
G2: 15.77%
S: 14.86%
G1/G0: 71.97%
G2: 13.75%
S: 14.28%
Cell Cycle
G0/G1 %
E
mAb04-MICA (nM) 0 0 200
VEGF (10ng/mL) - + +
p-VEGFR2
VEGFR2
p-AKT
AKT
β-Actin
F
mAb04-MICA (nM) 0 0 200
VEGF (10ng/mL) - + +
p-ERK
ERK
p-P38
P38
β-Actin
G
mAb04-MICA (nM) 0 200
Bax
Bak
Bcl-2
Bcl-xL
β-Actin

◂**Fig. 1** mAb04-MICA inhibited proliferation, promoted apoptosis, and altered cell cycle progression of tumor cells. **A**, mAb04-MICA bound to human tumor cell lines: AGS, BGC-823, and normal cell lines:HL-7702 by flow cytometry. **B**, mAb04-MICA, mAb04, and ramucirumab inhibited the proliferation of cell lines by MTT assay. **C**, BGC-823 cells and H157 cells were incubated with 200 nM mAb04 or mAb04-MICA at 37 °C for 72 h and analyzed by flow cytometry after staining with Annexin V-FITC and PI. Quantitative analysis is shown on the right. **D**, Representative images of cell cycle analysis by flow cytometry in BGC-823 cells and H157 cells that were incubated with mAb04 or mAb04-MICA. Quantitative analysis is shown on the right. **E**, western blot analysis for expressions of *p*-VEGFR2/VEGFR2, *p*-AKT/AKT, *p*-ERK/ERK, and *p*-P38/P38 by BGC-823 cells treated with VEGF with or without mAb-MICA. **F**, Expression of Bcl-2 family members Bax, Bak, Bcl-2, and Bcl-xl was examined by western blot. (Data are presented as the mean ± SD, $n = 3$, $^{*}p < 0.05$, $^{**}p < 0.01$, $^{***}p < 0.001$)

and CD49b (Cell Signaling). For immunofluorescence (IF) staining, tumor sections were incubated with anti-IFN-γ, anti-TNF-α, anti-iNOS, and anti-IL-2 antibodies (Abcam). Next, slides were mounted with Vectashield mounting media that contained DAPI and were analyzed under a fluorescence microscope.

Detection of the polarization and the cytokines of macrophage

RAW264.7 cells were treated as described in 2.6. Then, cells were detected the expression of CD16/32 (FcMRCS) and qPCR assay. PBMCs were obtained through density separation with Lymphocyte Separation Medium (Lympholyte®-H,Cedarlane). Briefly, 6 ml of diluted blood was carefully overlaid on 3 ml of lymphatic fluid ®-H and centrifuged at 800 g for 20 min at room temperature. After centrifugation, the cells were carefully removed from the interface and diluted with medium, and then, the lymphocytes were pelleted by centrifugation at 800 g for 10 min. The supernatant was discarded and washed 2–3 times in the medium. Isolated monocytes were then differentiated into macrophages by 7–9 days of culture in 1640 + 10% FBS supplemented with 10 ng/ml GM-CSF. Then, monocyte-derived human macrophages were treated in the same way as RAW264.7 cells for qPCR assay. Briefly, total RNA was extracted using TRIzol (Invitrogen). The cDNAs were synthesized from an equal amount of RNA (2 mg) using PrimeScript RT Master Mix (Takara) according to the manufacturer's instructions. SYBR Green mix (Roche) PCR amplification was performed using the Real-time PCR System. The primers were listed as Supplementary Table 2. The release of cytokines in the supernatant was detected through a TNF-α ELISA kit or DAF-FM DA.

Statistical analysis

The data were analyzed using GraphPad Prism. Results were presented as mean ± SD from at least three independent experiments. Significance levels were estimated using the Student's *t* test and *P* values of ≤ 0.05 were considered to be significant.

Results

mAb04-MICA inhibited proliferation, promoted apoptosis, and altered cell cycle progression of tumor cells

mAb04-MICA had strong binding with tumor cell lines BGC-823, AGS, H157, and H1299 (Fig. 1A, Fig. S1A), but little binding was seen with Normal cell lines HL7702, HEK-293. Knockdown of VEGFR2 on BGC-823 or H157 cells resulted in substantially reduced binding (Fig. S1A). Thus, mAb04-MICA exhibited VEGFR2-specific binding with tumor cells.

We observed that mAb04-MICA was more effective in inhibiting proliferation of GC cells and NSCLC cells than mAb04 and ramucirumab by MTT assays (Fig. 1B, Fig. S1B). After the VEGFR2 was depleted, the inhibition efficiency was almost lost. Meanwhile, little inhibition of proliferation of the HL-7702 was observed (Fig. S1B). These data show that mAb04-MICA bound specifically to tumor cells and inhibited their proliferation through VEGFR2.

The flow results showed that mAb04-MICA induced tumor cells apoptosis (Fig. 1C, Fig. S1C), and increased proportion of G0/G1 phase tumor cells (Fig. 1D, Fig. S1D). To further explore the antineoplastic mechanism, we detected the activation of VEGFR2 and the downstream signaling. Western blot analysis showed that mAb04-MICA inhibited VEGF-induced phosphorylation of VEGFR2/AKT/ERK/P38 MAPK (Fig. 1E, 1F, Fig. S1E, S1G–I). The expression of pro-apoptotic proteins Bak and Bax was increased and anti-apoptotic proteins Bcl-2/Bcl-xL were down-regulated (Fig. 1G, Fig. S1F, S1J–K). These results suggested that mAb04-MICA promoted apoptosis and altered cell cycle progression through weakening VEGFR2 dependent activation of AKT-ERK-P38 MAPK signaling.

mAb04-MICA enhanced antibody-dependent cellular cytotoxicity

To test the effect of mAb04-MICA on effector cell-mediated cytotoxicity, GC and NSCLC cells were co-cultured with PBMCs or NK-92 cells. PBMCs/tumor cells were 5:1, 30:1, and 100:1 and that of NK-92/tumor cells were 1:1, 5:1, and 10:1. We found that mAb04-MICA elicits greater cell lysis

than mAb04 (Fig. 2A–C). The specific lysis of tumor cells was reduced with free soluble MICA, which implied that free soluble MICA impaired the cytotoxicity of PBMCs and NK-92 cells. This is consistent with the literature that reported MICA shedding caused an immune escape [31, 32]. The activation of NK cells is evaluated by the expression of a degranulation marker CD107a. After co-incubated with BGC-823 cells treated with mAb04-MICA, the CD107a^{+} NK-92 cells were increased to 32.8%, and IFN-γ, TNF-α, granzyme B, and perforin production of NK-92 cells were enhanced (Fig. 2D–G). Similar results were observed in AGS cells (Fig. S2A-D). mAb04-MICA can enhance the

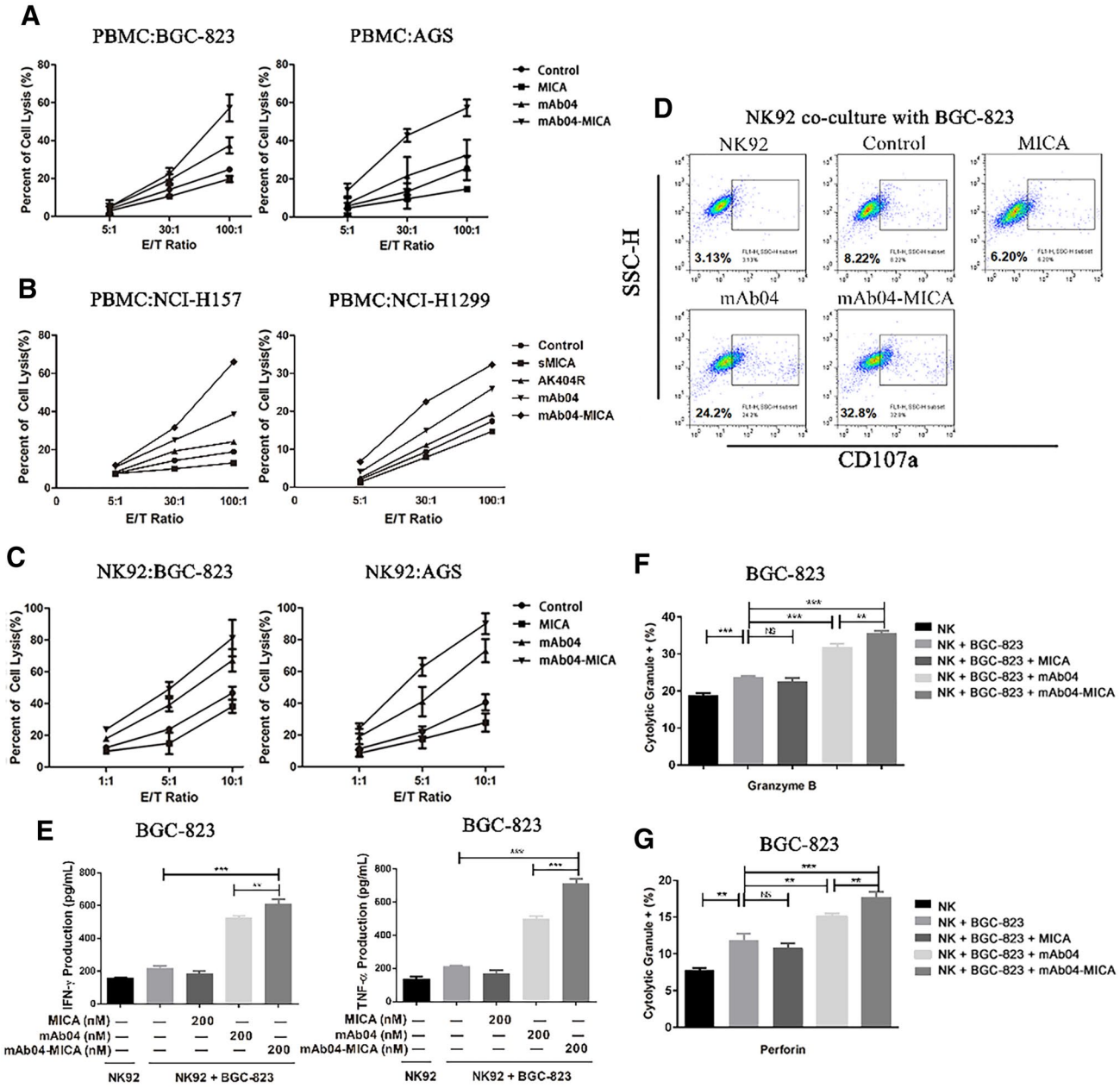

Fig. 2 mAb04-MICA enhanced the activation of NK cells in vitro. **A**, **B**, cytotoxicity assay to assess the PBMCs mediated killing of gastric cells BGC-823 and AGS cells, and NSCLC cells H157 and H1299. **C**, cytotoxicity assay to assess the NK-92 cell-mediated killing of BGC-823 and AGS cells. The E/T ratios of PBMCs/tumor cells were 5:1, 30:1, and 100:1 and that of NK-92/tumor cells were 1:1, 5:1, and 10:1. **D**, flow cytometry analysis of CD107a expression on NK-92 cells after exposure to BGC-823 cells with different treatments for 4 h. The E/T ratio was 10:1. **E**, ELISA assay for IFN-γ and TNF-α release after NK-92 cells were co-cultured with BGC-823 cells for 4 h at E/T ratio (10:1). F, G, quantitative analysis of perforin and granzyme B expression on NK-92 cells which was detected by flow cytometry after exposure to BGC-823 cells with different treatments for 4 h. The E/T ratio was 10:1. These experiments were repeated three times, and the data were presented as the mean ± SD, $*p<0.05$, $**p<0.01$, $***p<0.001$

activation of NK cells more effectively than mAb04 because of MICA.

mAb04-MICA showed superior anti-tumor efficacy

To evaluate the anti-tumor activity of mAb04-MICA in vivo, we used the GC (BGC-823,AGS) or NSCLC (H157)-bearing nude mice. The anti-tumor efficacy of mAb04-MICA treatment was superior to mAb04 and ramucirumab (Fig. 3A–H, Fig. S2E–H). Treatment with mAb04-MICA + docetaxel was more effective in inhibiting tumor growth than ramucirumab + docetaxel both in GC and NSCLC. (Fig. 3A–H, Fig. S2E-H. mAb04-MICA showed superior anti-tumor efficacy compared with ramucirumab both in single-dose treatments and when combined with docetaxel in vivo.

IHC demonstrated that the expression of proliferation marker Ki-67 was significantly decreased after treatment with mAb04-MICA. Meanwhile, decreased expression of VEGF and CD31 was also observed in mAb04-MICA and mAb04 group, which indicated the inhibition of tumor angiogenesis (Fig. 4A, Fig. S3A, S3B). There was no difference

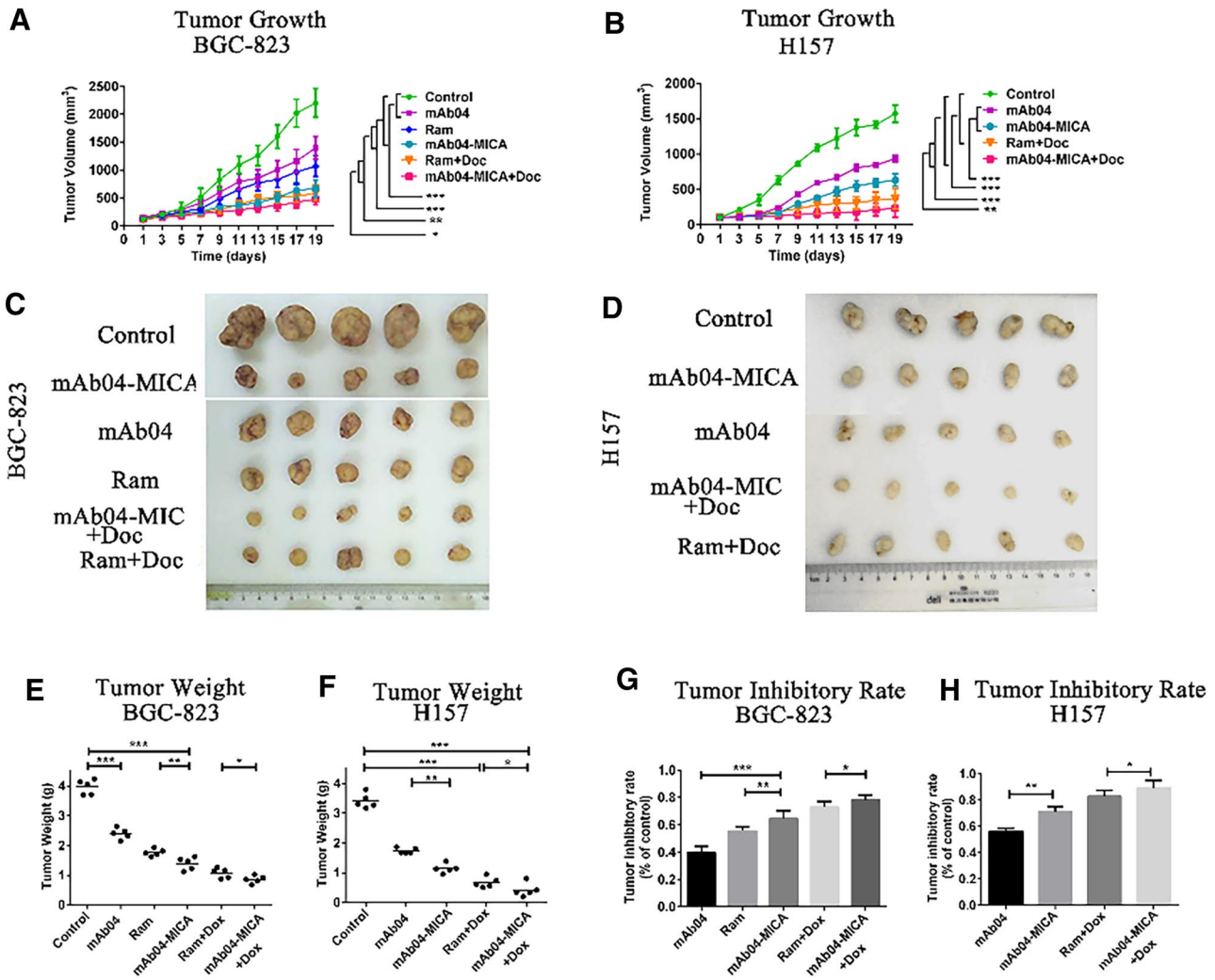

Fig. 3 mAb04-MICA had superior anti-tumor efficacy in cancer xenografts in vivo. **A**, **B**, tumor growth curves of each group under different treatments. 1×10^7 BGC-823 cells or H157 cells were injected subcutaneously into the left armpit of female BALB/c nude mice. When average tumor volume reached 100 $mm.^3$, tumor-bearing mice were treated with different treatments, and the tumor volume was measured. **C**, **D**, images of tumors peeled from different treatments in a BALB/c nude mice model. **E**, **F**, the average tumor weights of different groups after 19 d treatment. In the GC-bearing nude mice model, there were six groups: Control, mAb04-MICA (5 mg/kg), mAb04(5 mg/kg), ramucirumab (5 mg/kg), mAb04-MICA (5 mg/kg) + docetaxel (10 mg/kg), and ramucirumab (5 mg/kg) + docetaxel (10 mg/kg). In the NSCLC-bearing nude mice model, there were five groups: Control, mAb04-MICA (10 mg/kg), mAb04 (10 mg/kg), mAb04-MICA (10 mg/kg) + docetaxel (2 mg/kg), and ramucirumab (10 mg/kg) + docetaxel (2 mg/kg). G, H, the tumor inhibitory rate of BGC-823 and H157-bearing mice. Data were given as the mean ± SD ($n=5$). *$p<0.05$, **$p<0.01$, ***$p<0.001$

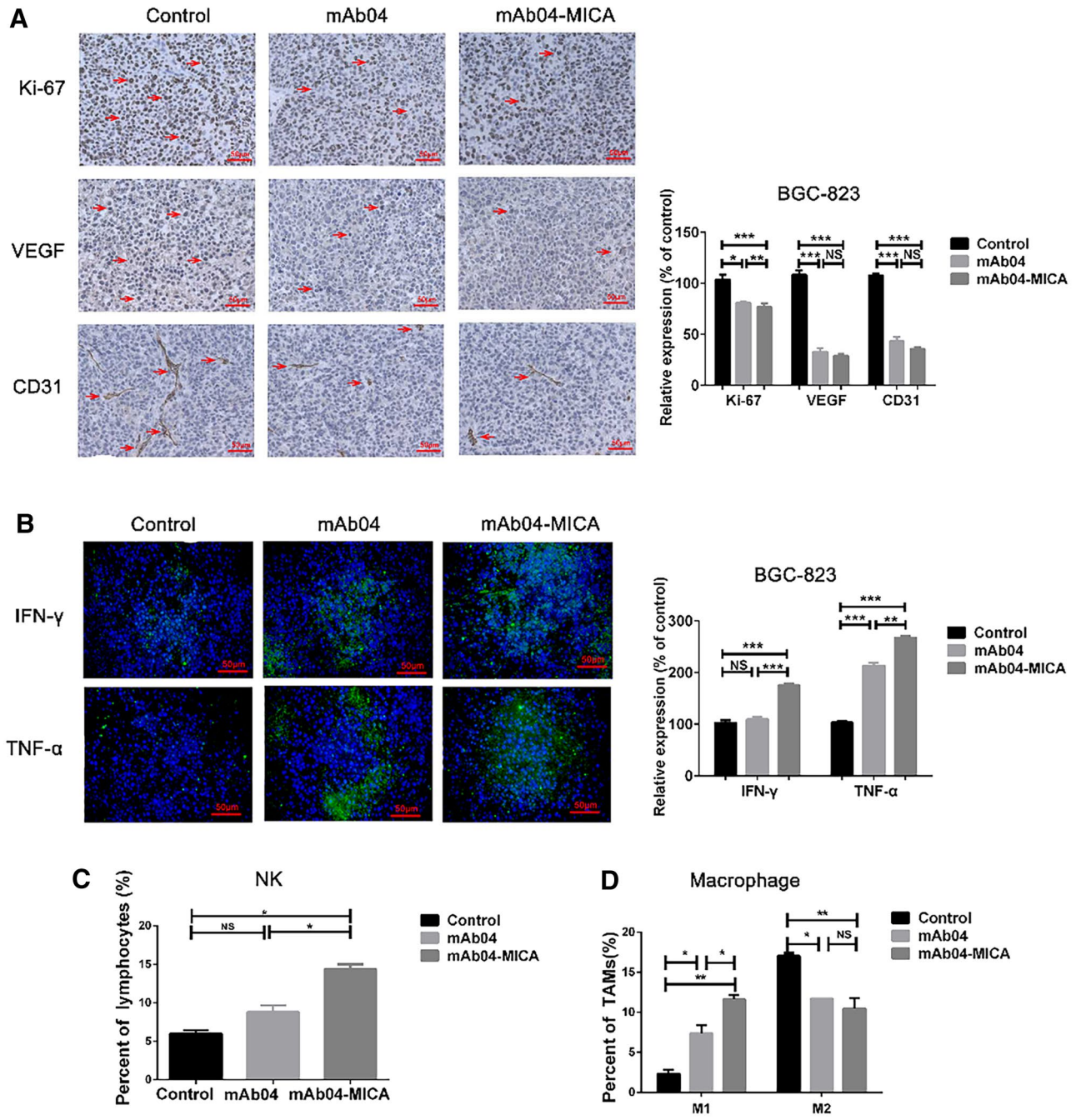

Fig. 4 mAb04-MICA reduced tumor cell proliferation and angiogenesis, and activated the innate immune system in tumor tissue. **A**, IHC staining of Ki-67, VEGF, and CD31 on paraffin sections in BGC-823 xenografted tumors. Positive cells were identified with antibodies in brown staining. Quantitative analysis is shown on the right. Ki-67 was counted with Image-Pro-Plus. Relative expression of Ki-67 (%) = (Experiment/Control) × 100%, and the formula is appropriate for calculating the relative expression of VEGF and CD31. Photomicrographs showed representative pictures from three independent tumor samples. Magnification, × 400. **B**, immunofluorescence staining to evaluate the levels of IFN-γ and TNF-α (green fluorescence) released in different groups. Magnification, × 400. Quantitative analysis is shown on the right. **C**, representative histogram (obtained from flow cytometry results) of frequency of $CD3^{-}CD49b^{+}$ NK cells in tumor tissue. **D**, representative histogram (obtained from flow cytometry results) of frequency of $F4/80^{+}CD16/32^{+}$ M1 macrophage and $F4/80^{+}CD206.^{+}$ M2 macrophage in tumor tissue. After administration for 10–12 d, mice were sacrificed, and the immune cells obtained from the tumor tissue were analyzed by flow cytometry. Data were presented as the mean ± SD, $n = 3$, $^{**}p < 0.01$, $^{***}p < 0.001$

of VEGF and CD31 between mAb04 and mAb04-MICA group. These results revealed that mAb04-MICA inhibited the proliferation of tumor cells more effectively than mAb04 not due to the inhibition of angiogenesis but resulted from the presence of MICA.

mAb04-MICA increased the infiltration and activation of immune cells in tumor tissue

To further explore the mechanism of the increased anti-tumor effects, we tested immune cells in tumor tissue. The results showed that mAb04-MICA significantly increased the expression of IFN-γ and TNF-α in tumor microenvironment (TME) compared with mAb04 treatment (Fig. 4B, Fig. S3C, S3D). In addition, $CD3^{-}CD49b^{+}$ NK cells were significantly increased after treatment with mAb04-MICA compared with mAb04, which indicated that mAb04-MICA exerted an anti-tumor effect by recruiting and activating NK cells (Fig. 4C). Notably, we found that the $CD16/32^{+}$ M1 state macrophage cells increased in the mAb04-MICA group compared with mAb04 treatment (Fig. 4D), which suggested a potential mechanism for MICA in the polarization of macrophages through NKG2D.

AK404R-MICA induced the polarization of RAW264.7 to M1 type

To understand the contribution of MICA-induced macrophage polarization and avoid the influence of crystallizable region (Fc), we used AK404R-MICA that consisted of an anti-VEGFR2 single-chain variable fragment (scFv) and MICAα1-α2. The biological activity of AK404R-MICA was like mAb04-MICA except for antibody-dependent cell-mediated cytotoxicity. The flow cytometry data revealed expression of the NKG2D protein in RAW264.7 cells (Fig. 5A), which indicated that RAW264.7 may be mediated through NKG2D and MICA.AK404R-MICA showed stronger cytotoxicity than AK404R in an E/T ratio-dependent manner (Fig. 5B) and the proportion of $CD16/32^{+}$ M1 macrophages increased when treated only with AK404R-MICA (Fig. 5C). Western blot analysis further showed increased expression of M1-specific CD16/32 and decreased expression of M2-specific CD206 (Fig. 5D). Meanwhile, RAW264.7 treated with AK404R-MICA contained higher gene expression levels of pro-inflammatory markers (TNF-α, iNOS, NO) when compared with non-polarized RAW264.7 and RAW264.7 treated with AK404R (Fig. 5C, E and F), which suggested that AK404R-MICA improved the polarization of RAW264.7 to M1 through MICA. The macrophage RAW264.7 polarized toward pro-tumor 'M2' state treatment with IL4 [33]. It is noticed that similar results were observed with RAW264.7 treated with IL4 and monocyte-derived human macrophages treated with IL4 (Fig. S3H, S3I). These findings revealed a new mechanism on how MICA reprogrammed TAM by inducing polarization of macrophages to M1 and reversing the M2–M1 macrophage.

AK404R-MICA showed superior anti-tumor efficacy

To assess the action of NKG2D-MICA in immune-competent mice, we subcutaneously transplanted LLC cells in C57BL/6 mice. The anti-tumor effect of AK404R-MICA was assessed by tumor growth, tumor volume, tumor weight, and tumor-inhibiting rate (Fig. 6A-D). We observed that AK404R-MICA attenuated tumor growth compared with AK404R group and control group. AK404R-MICA and AK404R treatment showed 77.01% and 60.93% inhibition of tumor weight, respectively (Fig. 6D). The toxicity was evaluated by the spleen index and liver index. AK404R-MICA treatment showed no significant difference compared with control group (Fig. 6E, 6F).

To confirm AK404R-MICA-induced anti-tumor effect by modulating TIME, TILs were extracted from tumors and analyzed by flow. $CD3^{-}CD49b^{+}$ NK cells intra-tumoral infiltration increased significantly after treatment with AK404R-MICA, but there was no significant difference between the AK404R group and control group. Similar data were observed in $CD3^{+}CD8^{+}$T cells (Fig. 6G). Under AK404R-MICA treatment, a significant increase in $CD107a^{+}$ NK and $CD69^{+}CD8^{+}$T cells indicated that there was an increase in activated NK and $CD8^{+}$T cells, respectively (Fig. 6H). In the $NKG2D^{+}$ macrophage subclass, increased CD16/32 and reduced CD206 suggested that AK404R-MICA treatment led to an increase in M1 and a decrease in M2 macrophages (Fig. 6I).

The IHC and immunofluorescence assay confirmed above findings. IHC revealed that NK cells and $CD8^{+}$T cells were recruited to the tumor tissues after AK404R-MICA treatment (Fig. 6J, 6K). Immunofluorescence showed that the release of IFN-γ, IL-2, iNOS significantly increased in the AK404R-MICA group (Fig. 6L). This certified our findings that anti-VEGFR2-MICA can exert excellent anti-tumor efficacy through activating NK cells, $CD8^{+}$T cells, and improving the polarization of macrophages to M1.

Combination treatment reprogramed the immune microenvironment

mAb04-MICA can increase the expression of PD-L1 in tumor tissues (Fig. 7A), we studied whether PD-1 blockade improves the anti-tumor activity of mAb04-MICA. The combination of the anti-PD-1 antibody JZD00 and mAb04-MICA further improved tumor growth control in the H1975-bearing nude mouse (Fig. 7B–D). We studied the mechanism in an NSCLC-bearing NOD-SCID model. More activated $CD107a^{+}CD56^{+}$NK cells infiltrated into

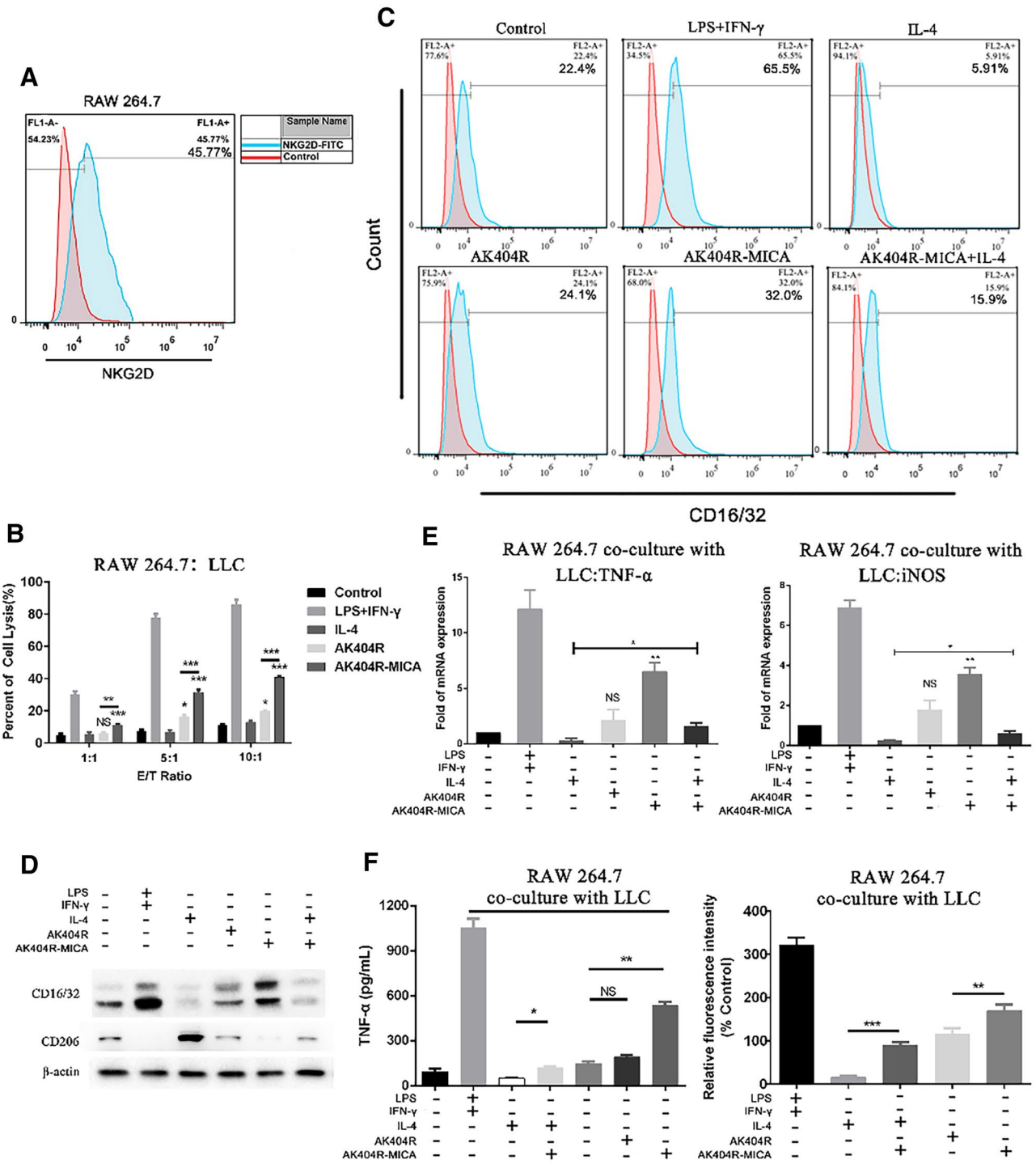

Fig. 5 AK404R-MICA induced the polarization of macrophages to M1 type in vitro. **A**, expression of NKG2D on RAW 264.7 detected by flow cytometry. RAW 264.7 was co-cultured with LLC for 24 h before detection. RAW 264.7 cells were co-cultured with LLC for 24 h with 5 ng/mL IFN-γ + 100 ng/mL LPS,10 ng/mL IL-4, 1000 nM AK404R or AK404R-MICA for another 48 h, respectively. Then culture supernatant and the cells were harvested to analysis: **B**, cytotoxicity assay to assess the RAW 264.7 cell-mediated killing of LLC cells by LDH release assay. **C**, flow cytometry detected the proportion of CD16/32.$^{+}$ M1 type macrophages under different conditions. **D**, western blot analysis for the CD16/32 and CD206 for M1 and M2 type macrophages respectively. **E**, qPCR analysis for TNF-α and iNOS released by M1 macrophages. **F**, left, the release of TNF-α detected by ELISA. Right, the release of NO detected by DAF-FM DA. Data were presented as the mean ± SD, $n = 3$, $^{**}p < 0.01$, $^{***}p < 0.001$

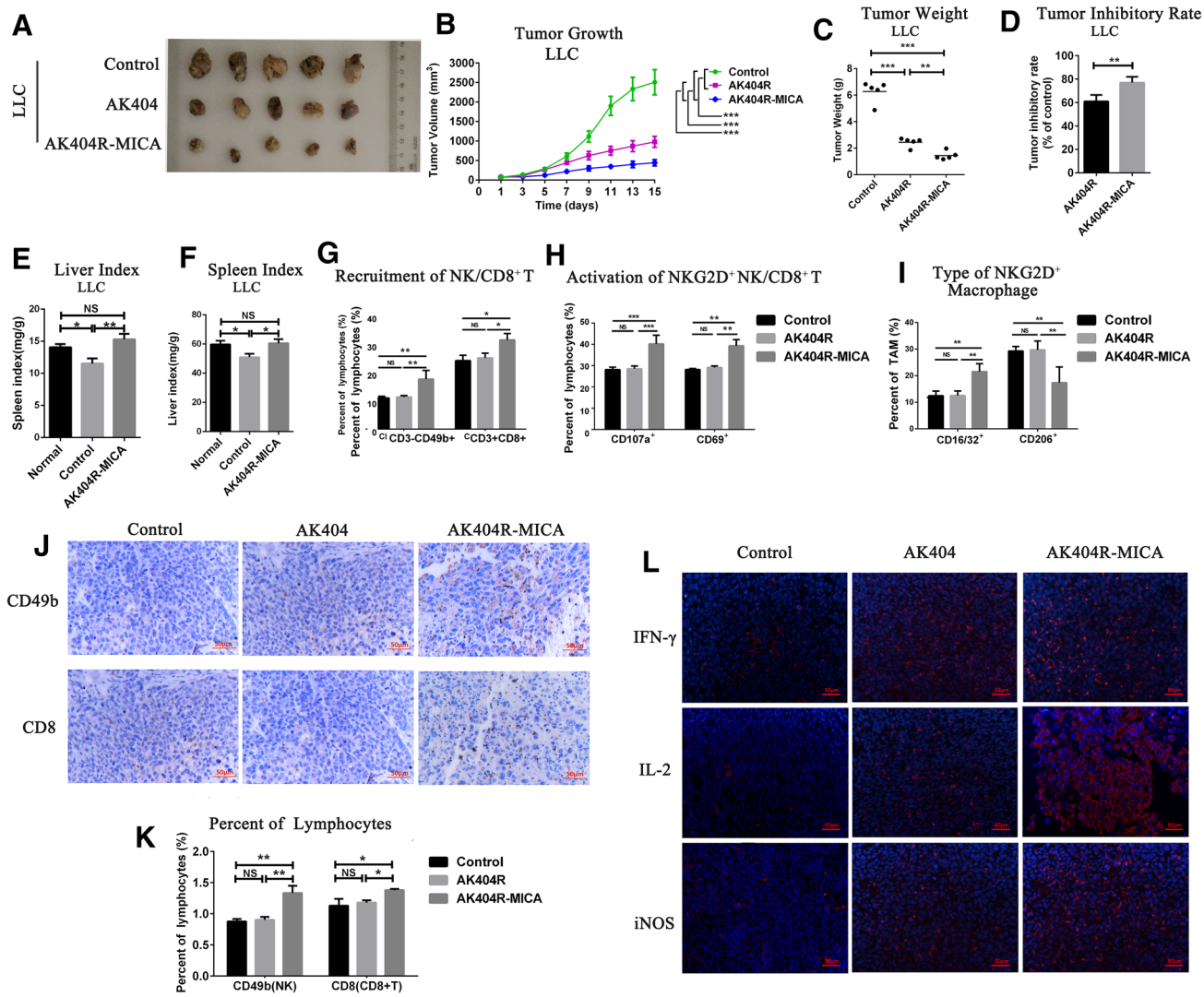

Fig. 6 AK404R-MICA showed superior anti-tumor efficacy in LLC model in vivo through recruiting and activating immune cells and inducing the polarization of macrophages to M1 type. **A**, tumor images of each group under different treatments after 15d. **B**, growth curves of tumors. **C**, the average tumor weights of different groups. **D**, Tumor inhibitory rate of different groups. Data were given as the mean ± SD ($n=5$). *$p<0.05$, **$p<0.01$, ***$p<0.001$. **E**, **F**, the liver index and spleen index of AK404R-MICA compared with normal mice. Liver index/spleen index (mg/g) = Liver/Spleen weight (mg)/Mice weight (g). **G**, **H**, quantitative analysis of recruitment and activation of NKG2D$^+$ NK (CD3$^-$CD49b$^+$CD107a$^+$) cells and T (CD3$^+$CD8$^+$CD69$^+$) cells. **I**, quantitative analysis of polarization of NKG2D$^+$ macrophage cells to M1 (F4/80$^+$CD16/32$^+$) phenotype or M2 (F4/80$^+$CD206$^+$) phenotype. **J**, IHC staining of CD49b and CD8 on paraffin sections that represents NK cells and CD8$^+$ T cells in LLC xenografted tumors. Positive cells were identified with antibodies in brown staining. Magnification, ×400. **K**, semiquantitative and statistical analysis of CD49b$^+$ NK cells and CD8$^+$ T cells. **L**, immunofluorescence staining to evaluate the levels of IFN-γ, IL-2, and iNOS (red fluorescence) that were released by NK cells, CD8.$^+$ T cells, and macrophage cells. (Green fluorescence) in different groups. Magnification, ×400

tumors in the combination treatment group (Fig. 7E–F, Fig. S3A–B). Following blockade of PD-1, tumor-infiltrating CD8$^+$T cells showed improved function in SCID mice, as indicated by the increased frequency of such cells expressing IFN-γ (Fig. 7G–I; Fig. S3C-D). PD-1 blockade reduced the number of CD4$^+$Foxp3$^+$Treg cells and increased the number of CD4$^+$Foxp3$^-$ cells, thus reversing the immunosuppressed TME (Fig. 7J; Fig. S3E). The results were further confirmed in expression of cytokines (Fig. 7K). JZD00 and mAb04-MICA alone significantly promoted the release of the activating cytokines IFN-γ and IL-2 but had no significant effect on the inhibitory factors Foxp3 and TGF-β. When combined, the release of activating factors was further increased, while the expression of inhibitory factors was significantly decreased (Fig. 7K). Combination therapy trended to reduce blood permeability and HIF-1α expression in tumor tissue (Fig. 7L–M), which suggested that the degree of blood vessels normalization was increased.

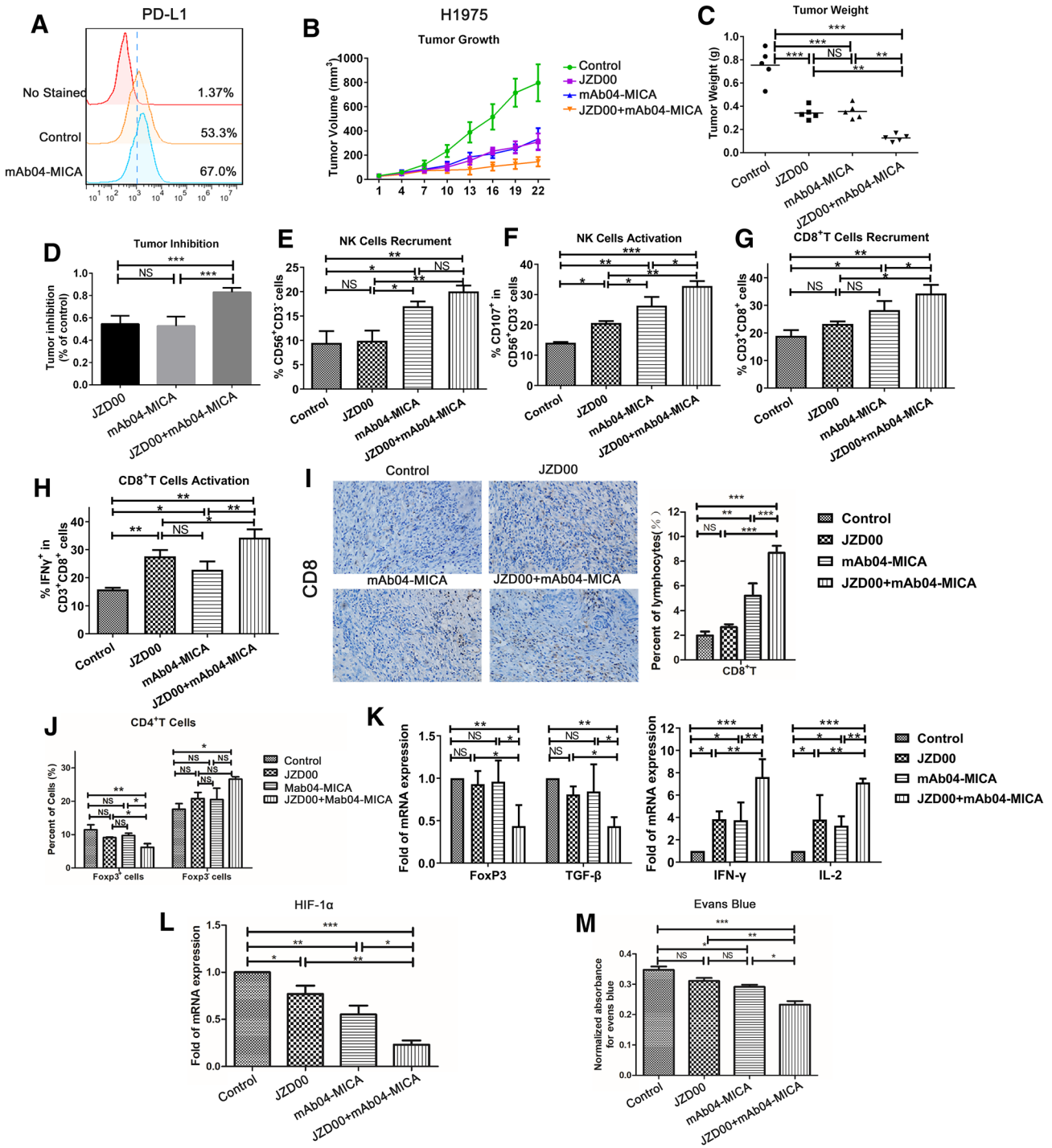

Fig. 7 Anti–PD-L1 enhances the anti-tumoral activity of Mab04-MICA in NSCLC model through stimulating infiltration and activation of NKs and CTLs in responding tumors. **A** After mAb04-MICA treatment, the expression of PD-L1 in tumor tissues was detected by flow cytometry. **B** Subcutaneous tumor growth curve of H1975 human non-small cell lung cancer mice, **C** tumor weight, **D** tumor inhibition rate. ($N=5$). Data were given as the mean ± SD ($n=5$). $*p<0.05$, $**p<0.01$, $***p<0.001$. **E**–**J**, Recruitment and activation of NKs and CTL in tumor tissue. **A** NOD-SCID mouse xenografted tumor model of human non-small cell lung cancer was established. After 4–5 doses, flow cytometry was used to detect the infiltration rate of $CD56^+$NK cells(E), number of activated CD107a + CD56 + NK cells(F), CD8 + T cell infiltration level(G), activated IFN-γ + CD8 + T cells(H) in tumor tissues. *I*. Immunohistochemical detection of infiltrating CD8 + T cells in tumor tissues and statistical analysis. **J**, CD4 + Foxp3 + Treg and CD4 + Foxp3-Treg. **K**, the release of Foxp3, TGF-β, IFN-γ, IL-2, HIF-1α, and other cytokines was detected by qPCR. **M**, Evans Blue detects the degree of vascular leakage

Discussion

We have introduced and validated tumor-targeted immunotherapy using a mAb04-MICA bi-specific fusion protein. mAb04-MICA directly killed cancer cells, induced anti-tumor immunity through intra-tumoral NK and T cell infiltration and activation, and inhibited tumor angiogenesis. Moreover, mAb04-MICA-induced polarization of macrophages from M2 to M1. The release of cytokines such as TNF-α, IFN-γ, IL-2, and iNOS was also elevated. In addition, PD-1 blockade improved the anti-tumoral activity of mAb04-MICA and improved the tumor immunosuppressive microenvironment. Thus, our findings highlight the importance of combining an antiangiogenic regimen with a PD-1 blockade to stimulate superior anti-tumor effects. (Fig. 8).

NKG2D-mediated immune surveillance plays a pivotal role in inhibiting tumorigenesis and tumor progression [34, 35]. However, advanced cancers frequently shed MICA to prevent recognition by immune cells, leading to immune escape. The main challenge of reestablishing tumor immunity is the restoration of NKG2D surveillance [36, 37]. One approach has been to create antibodies against MICA, thereby blocking the site of proteolytic shedding [21]. This strategy achieved positive results in MICA over-expressed tumor cells. However, the efficacy of antibodies against MICA might have limited efficiency for patients with low shed MICA or advanced cancers. Another approach attempted to induce the tumor cells to re-express NKG2D ligands through a stimulating factor, such as IL-2 and doxorubicin [38]. Although this strategy showed a promising anti-tumor effect, there is the potential for cytotoxicity when considering clinical use. mAb04-MICA was designed to both restore NKG2D immunosurveillance and inhibit angiogenesis. Recognition and targeting of tumor cell VEGFR2 allow MICA to be localized in tumor tissues. This results in recruitment of NKG2D positive immune cells and activation of antibody-dependent cellular cytotoxicity.

We found that mAb04-MICA can strongly bind to tumor cells and inhibit their proliferation through the VEGFR2 pathway. Based on the strong ability to target VEGFR2, we also studied whether MICA was able to simultaneously restore immune surveillance by recruiting and activating NK cells in the tumor microenvironment. In vitro, the killing effects of NK-92 cells and PBMCs were enhanced after treatment with mAb04-MICA. This was supported by the secretion of IFN-γ and TNF-α increased significantly and the release of granzyme B and perforin were elevated. In vivo, the proportion of NK cells and the release of IFN-γ and TNF-α were increased significantly in tumor tissues after mAb04-MICA treatment, reinforcing its ability to activate NK cells. Additionally, an increase of activated $CD8^+$T cells was also detected in tumor tissue.

Macrophages are also reported to express NKG2D [23]. Tumor cells use their negative regulatory pathways to establish a tumor immunosuppressive microenvironment, especially by down-regulating MICA. M1 Macrophages are a critical component of immune recognition and destruction of tumor cells. M2 macrophages differentiate into M1 macrophages through the interaction of MICA on tumor cells

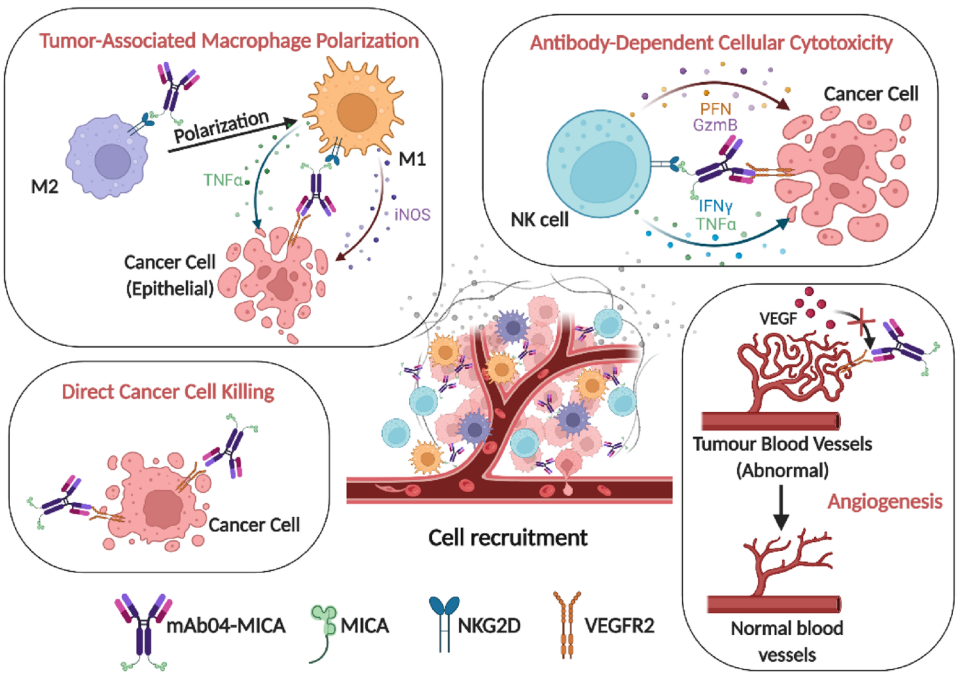

Fig. 8 Illustration of mAb04-MICA and AK404R-MICA: structure and therapeutic mechanisms

[39, 40]. It is therefore of importance to restore MICA in the tumor environment to increase M1 macrophages in cancer treatment [40]. Interestingly, mAb04-MICA was found to have this capability through its ability to resupply M1 macrophages with MICA stimulation and activation in the tumor microenvironment.

To elucidate the molecular mechanism and remove the impact of Fc fragment, we designed a smaller format using the scFv of mAb04 (AK404R-MICA). In vitro, the killing effect of RAW264.7 on LLC was enhanced after AK404R-MICA treatment. A significant increase of M1 macrophages were seen after AK404R-MICA treatment. This was consistent with the increased expression of M1 macrophage-specific cytotoxic genes TNF-α and iNOS at the protein and mRNA level. AK404R-MICA treatment can reverse the induced RAW264.7 cells from M2 to M1 to some extent. In vivo, AK404R-MICA induced an increased polarization of M2 macrophages to M1. These findings offer a comprehensive understanding of how AK404R-MICA interacts with the innate immune system.

PD-1/PD-L1 expression has been reported to be up-regulated during antiangiogenic therapy, resulting in increased tumor-adaptive immunosuppression despite increased lymphocyte infiltration [41]. GC patients treated with ramolumab showed increased $CD8^+$T cell infiltration and up-regulation of PD-L1 levels [42]. mAb04-MICA therapy alone induced the up-regulation of PD-L1 expression in tumor tissues. It is speculated that mAb04-MICA may lead to the increased release of IFN-γ, which can regulate the expression of PD-L1 in tumor tissues [40]. When JZD00 was combined with mAB04-MICA, the degree of NK cell activation was significantly increased. This is likely explained by the synergistic effect of MICA/NKG2D engagement and the inability of tumor cell PD-L1 to engage with NK PD-1. mAb04-MICA can recruit $CD8^+$T cells, but activation cannot be initiated unless PD-1/PD-L1 engagement with tumor cells is disrupted. Therefore, after blocking PD-1, the activation of $CD8^+$T cells increased, and the release of IFN-γ and IL-2 was promoted. Additionally, JZD00 and mAb04-MICA alone had no significant effect on inhibitory factors Foxp3 and TGF-β. When combined with mAb04-MICA, the release of activating factors was increased, while the expression of inhibitory factors was significantly decreased, indicating that the immune microenvironment was significantly activated.

mAb04-MICA showed better anti-tumor effects in vivo, compared with either ramucirumab alone in combination with docetaxel in GC and NSCLC models. We suspect that mAb04-MICA reduced drug resistance through the activation of the innate immune system. Although mAb04-MICA has cross-reactivity with murine VEGFR2 (Fig. S3G), no significant side effect was observed in a primary cytotoxicity assay. Still, the chronic toxicity of mAb04-MICA treatment needs to be investigated in a primate model.

In summary, our study demonstrated that mAb04-MICA has multifunctional modulating activity on innate immune systems. Dual targeting of angiogenesis and NKG2D displays better efficacy in solid tumors than single targeting alone. This work shows strong evidence that the tumor-suppressive immune microenvironment can be reversed and that the strategy of using a MICA-fused antibody can be further applied to other tumor-specific antigens. This behavior suggests promising therapeutic advances to the current therapeutic antibodies used in clinical practice, and it provides innovative thought for the new generation of cancer immunotherapy. However, poor tissue penetration remains a major challenge for full-length antibody-based therapeutics of solid tumors. Several studies have made progress in addressing the problem of tissue penetration of large proteins. The researchers find that co-administration of the parent antibody with the antibody–dye conjugate significantly improved the distribution of the antibody–dye conjugate in human patients while lowering uptake in healthy tissue [43]. In addition, tumor-penetrating peptide, iRGD (CRGDK/RGPD/EC), increased vascular and tissue permeability in a tumor-specific and neuropilin-1-dependent manner, allowing co-administered drugs to penetrate into extravascular tumor tissue [44]. The combination of these methods will further increase the anti-tumor efficacy and safety of the antibody.

Supplementary Information The online version contains supplementary material available at https://doi.org/10.1007/s00262-022-03306-1.

Author contributions All authors contributed to the study conception and design. MP and FW designed and performed the experiments, carried out statistical analysis, and wrote the manuscript. LN guided anti-tumor efficacy in LLC model. SY, JQ, and HZ performed antibody-dependent cellular cytotoxicity assay, MTT assay, and helped with anti-tumoral activity in NSCLC model. JX and SS performed immunohistochemistry, PubMed searches and edited the manuscript. JZ proposed the study design, conducted the study supervision, and revised the manuscript. FS performed analysis and interpretation of data, and revised the manuscript. MW reviewed and revised the manuscript. All authors read and approved the final manuscript.

Funding This work was supported by the National Natural Science Foundation (NSFC81973223), and the National College Students Innovation and Entrepreneurship Training Program (202210316062Y, China).

Declarations

Conflict of interest The authors declare no potential conflicts of interest.

References

1. Otrock ZK, Makarem JA, Shamseddine AI (2007) Vascular endothelial growth factor family of ligands and receptors: review. Blood Cells Mol Dis 38(3):258–268
2. Shibuya M, Claesson-Welsh L (2006) Signal transduction by VEGF receptors in regulation of angiogenesis and lymphangiogenesis. Exp Cell Res 312(5):549–560

3. Xuan ZX, Li LN, Zhang Q, Xu CW, Yang DX, Yuan Y et al (2014) Fully human VEGFR2 monoclonal antibody BC001 attenuates tumor angiogenesis and inhibits tumor growth. Int J Oncol 45(6):2411–2420
4. Folkman J (1971) Tumor angiogenesis: therapeutic implications. N Engl J Med 285(21):1182–1186
5. Ferrara N, Adamis AP (2016) Ten years of anti-vascular endothelial growth factor therapy. Nat Rev Drug Discov 15(6):385–403
6. Fuchs CS, Tomasek J, Yong CJ, Dumitru F, Passalacqua R, Goswami C et al (2014) Ramucirumab monotherapy for previously treated advanced gastric or gastro-oesophageal junction adenocarcinoma (REGARD): an international, randomised, multicentre, placebo-controlled, phase 3 trial. Lancet 383(9911):31–39
7. Wilke H, Muro K, Van Cutsem E, Oh SC, Bodoky G, Shimada Y et al (2014) Ramucirumab plus paclitaxel versus placebo plus paclitaxel in patients with previously treated advanced gastric or gastro-oesophageal junction adenocarcinoma (RAINBOW): a double-blind, randomised phase 3 trial. Lancet Oncol 15(11):1224–1235
8. Garon EB, Ciuleanu TE, Arrieta O, Prabhash K, Syrigos KN, Goksel T et al (2014) Ramucirumab plus docetaxel versus placebo plus docetaxel for second-line treatment of stage IV non-small-cell lung cancer after disease progression on platinum-based therapy (REVEL): a multicentre, double-blind, randomised phase 3 trial. Lancet 384(9944):665–673
9. Roodhart JM, Langenberg MH, Witteveen E, Voest EE (2008) The molecular basis of class side effects due to treatment with inhibitors of the VEGF/VEGFR pathway. Curr Clin Pharmacol 3(2):132–143
10. Nandikolla AG, Rajdev L (2016) Targeting angiogenesis in gastrointestinal tumors: current challenges. Trans Gastroenterol Hepatol 1:67
11. Arnold D, Fuchs CS, Tabernero J, Ohtsu A, Zhu AX, Garon EB et al (2017) Meta-analysis of individual patient safety data from six randomized, placebo-controlled trials with the antiangiogenic VEGFR2-binding monoclonal antibody ramucirumab. Ann Oncol 28(12):2932–2942
12. Jung K, Heishi T, Incio J, Huang Y, Beech EY, Pinter M et al (2017) Targeting CXCR4-dependent immunosuppressive Ly6C(low) monocytes improves antiangiogenic therapy in colorectal cancer. Proc Natl Acad Sci U S A 114(39):10455–10460
13. Jenkins RW, Barbie DA, Flaherty KT (2018) Mechanisms of resistance to immune checkpoint inhibitors. Br J Cancer 118(1):9–16
14. Lanier LL (2005) NK cell recognition. Annu Rev Immunol 23:225–274
15. Long EO, Kim HS, Liu D, Peterson ME, Rajagopalan S (2013) Controlling natural killer cell responses: integration of signals for activation and inhibition. Annu Rev Immunol 31:227–258
16. Nakamura K, Nakayama M, Kawano M, Amagai R, Ishii T, Harigae H et al (2013) Fratricide of natural killer cells dressed with tumor-derived NKG2D ligand. Proc Natl Acad Sci U S A 110(23):9421–9426
17. López-Soto A, Huergo-Zapico L, Acebes-Huerta A, Villa-Alvarez M, Gonzalez S (2015) NKG2D signaling in cancer immunosurveillance. Int J Cancer 136(8):1741–1750
18. Nausch N, Cerwenka A (2008) NKG2D ligands in tumor immunity. Oncogene 27(45):5944–5958
19. Ghadially H, Brown L, Lloyd C, Lewis L, Lewis A, Dillon J et al (2017) MHC class I chain-related protein A and B (MICA and MICB) are predominantly expressed intracellularly in tumour and normal tissue. Br J Cancer 116(9):1208–1217
20. Schilling D, Kühnel A, Tetzlaff F, Konrad S, Multhoff G (2015) NZ28-induced inhibition of HSF1, SP1 and NF-κB triggers the loss of the natural killer cell-activating ligands MICA/B on human tumor cells. Cancer Immunol, Immunother : CII 64(5):599–608
21. de Ferrari Andrade L, Tay RE (2018) Antibody-mediated inhibition of MICA and MICB shedding promotes NK cell–driven tumor immunity. Science 359(6383):1537–1542
22. Wang T, Sun F, Xie W, Tang M, He H, Jia X et al (2016) A bispecific protein rG7S-MICA recruits natural killer cells and enhances NKG2D-mediated immunosurveillance against hepatocellular carcinoma. Cancer Lett 372(2):166–178
23. Strong RK, McFarland BJ (2004) NKG2D and related immunoreceptors. Adv Protein Chem 68:281–312
24. Gordon SR, Maute RL, Dulken BW, Hutter G, George BM, McCracken MN et al (2017) PD-1 expression by tumour-associated macrophages inhibits phagocytosis and tumour immunity. Nature 545(7655):495–499
25. Wang X, Luo G, Zhang K, Cao J, Huang C, Jiang T et al (2018) Hypoxic tumor-derived exosomal miR-301a mediates M2 macrophage polarization via PTEN/PI3Kγ to promote pancreatic cancer metastasis. Cancer Res 78(16):4586–4598
26. Mantovani A, Sozzani S, Locati M, Allavena P, Sica A (2002) Macrophage polarization: tumor-associated macrophages as a paradigm for polarized M2 mononuclear phagocytes. Trends Immunol 23(11):549–555
27. Xie W, Liu F, Wang Y, Ren X, Wang T, Chen Z et al (2016) VEGFR2 targeted antibody fused with MICA stimulates NKG2D mediated immunosurveillance and exhibits potent anti-tumor activity against breast cancer. Oncotarget 7(13):16445–16461
28. Xu Y, Zhang XR, Wang Y, Pan MZ, Wang M, Zhang J (2019) A VEGFR2-MICA bispecific antibody activates tumor-infiltrating lymphocytes and exhibits potent anti-tumor efficacy in mice. Cancer Immunol Immun 68(9):1429–1441
29. Moffat J, Grueneberg DA, Yang X, Kim SY, Kloepfer AM, Hinkle G et al (2006) A lentiviral RNAi library for human and mouse genes applied to an arrayed viral high-content screen. Cell 124(6):1283–1298
30. Alter G, Malenfant JM, Altfeld M (2004) CD107a as a functional marker for the identification of natural killer cell activity. J Immunol Methods 294(1–2):15–22
31. Groh V, Wu J, Yee C, Spies T (2002) Tumour-derived soluble MIC ligands impair expression of NKG2D and T-cell activation. Nature 419(6908):734–738
32. Klöß S, Chambron N, Gardlowski T, Arseniev L, Koch J, Esser R et al (2015) Increased sMICA and TGFβ(1) levels in HNSCC patients impair NKG2D-dependent functionality of activated NK cells. Oncoimmunology 4(11):e1055993
33. Lee SJ, Lim KT (2008) Phytoglycoprotein inhibits interleukin-1β and interleukin-6 via p38 mitogen-activated protein kinase in lipopolysaccharide-stimulated RAW 264.7 cells. Naunyn-Schmiedeberg's Arch Pharmacol 377(1):45–54
34. Waldhauer I, Steinle A (2008) NK cells and cancer immunosurveillance. Oncogene 27(45):5932–5943
35. Pahl J, Cerwenka A (2017) Tricking the balance: NK cells in anticancer immunity. Immunobiology 222(1):11–20
36. Schmiedel D, Mandelboim O (2018) NKG2D Ligands-critical targets for cancer immune escape and therapy. Front Immunol 9:2040
37. Deguine J, Breart B, Lemaître F, Bousso P (2012) Cutting edge: tumor-targeting antibodies enhance NKG2D-mediated NK cell cytotoxicity by stabilizing NK cell-tumor cell interactions. J Immunol 189(12):5493–5497
38. Hu J, Bernatchez C, Zhang L, Xia X, Kleinerman ES, Hung MC et al (2017) Induction of NKG2D ligands on solid tumors requires tumor-specific CD8(+) T cells and histone acetyltransferases. Cancer Immunol Res 5(4):300–311
39. Alexander ET, Minton AR, Peters MC, van Ryn J, Gilmour SK (2016) Thrombin inhibition and cisplatin block tumor progression

in ovarian cancer by alleviating the immunosuppressive microenvironment. Oncotarget 7(51):85291–85305
40. Sica A, Schioppa T, Mantovani A, Allavena P (2006) Tumour-associated macrophages are a distinct M2 polarised population promoting tumour progression: potential targets of anti-cancer therapy. Eur J Cancer 42(6):717–727
41. Allen E, Jabouille A (2017) Combined antiangiogenic and anti–PD-L1 therapy stimulates tumor immunity through HEV formation. Sci Trans Med 9(385):eaak9679
42. Tada Y, Togashi Y, Kotani D, Kuwata T, Sato E, Kawazoe A et al (2018) Targeting VEGFR2 with Ramucirumab strongly impacts effector/ activated regulatory T cells and CD8(+) T cells in the tumor microenvironment. J Immunother Cancer 6(1):106
43. Lu G, Nishio N, van den Berg NS, Martin BA, Fakurnejad S, van Keulen S et al (2020) Co-administered antibody improves penetration of antibody-dye conjugate into human cancers with implications for antibody-drug conjugates. Nat Commun 11(1):5667
44. Sugahara KN, Teesalu T, Karmali PP, Kotamraju VR, Agemy L, Greenwald DR et al (2010) Coadministration of a tumor-penetrating peptide enhances the efficacy of cancer drugs. Science 328(5981):1031–1035